J-RA/4/3//20157

Direct-Drive Active Complaint End Effector (Active RCC)

H. Kazerooni

Reprinted from
IEEE JOURNAL OF ROBOTICS AND AUTOMATION
Vol. 4, No. 3, June 1988

Direct-Drive Active Compliant End Effector (Active RCC)

H. KAZEROONI

Abstract—A fast, lightweight, active end effector which can be attached to the endpoint of a commercial robot manipulator has been designed and built. Impedance control [11] has been developed on this device. This control method causes the end effector to behave dynamically as a two-dimensional Remote Center Compliance (RCC). The compliancy in this active end effector is electronic and so can be modulated by an on-line computer.

The device is a planar, five-bar linkage which is driven by two direct-drive, brushless dc motors. A two-dimensional, piezoelectric force cell on the endpoint of the device, two 12-bit encoders, and two tachometers on the motors form the measurement system. The high structural stiffness and light weight of the material used in the system allow for a 15-Hz bandwidth impedance control.

Nomenclature

E	Environment dynamics.
e	Input trajectory.
F	Contact force.
G	Closed-loop transfer function matrix.
H	The compensator.
j	Complex number notation $\sqrt{-1}$.
J_0	Jacobian.
j_i	Moment of inertia of each link relative to the endpoint of the link.
K	Stiffness matrix.
K_n, K_t	Stiffness in the direction normal and tangential to the part.
l_i, m_i	Length and mass of each link.
M_0	Inertia matrix.
M	The grinder mass in the passive end effector.
S	Sensitivity transfer function matrix.
r	Input command vector.
$T = [T_1\ T_2]^T$	Torque vector.
$X = [X_t\ X_n]^T$	Vector of the tool position in the Cartesian coordinate frame.
X_0	Environment position measured in the Cartesian coordinate frame.
x_i, θ_i	Location of the center of mass and orientation of each link.
α	Small perturbation of θ_1 in the neighborhood of $\theta_1 = 90°$.
δe	Endpoint deflection in X_n direction.
δX_n, δX_t	Endpoint deflection in the direction normal and tangential to the part.
δF_n, δF_t	Contact force in the direction normal and tangential to the part.
ω_b	Frequency range of the burr observed from the robot endpoint.
ω_d	Dynamic manipulability.
ω_o	Frequency range of the operation (bandwidth).
ω_r	Frequency range of the robot oscillations.

Manuscript received January 12, 1987; revised October 6, 1987.

The author is with the Mechanical Engineering Department, University of Minnesota, Minneapolis, MN 55455.

IEEE Log Number 8820157.

I. Introduction

MANUFACTURING manipulations require mechanical interaction with the environment or with the object being manipulated. Robot manipulators are subject to interaction forces when they maneuver in a constrained workspace. Inserting a computer board in a slot or deburring an edge are examples of constrained maneuvers. In constrained maneuvers, one is concerned with not only the position of the robot endpoint, but also the contact forces. In constrained maneuvering, the interaction forces must be accommodated rather than resisted. If we define compliancy as a measure of the ability of the manipulators to react to interaction forces and torques, the objective is to assure compliant motion (passively or actively) for the robot endpoint in the Cartesian coordinate frame for manipulators that must maneuver in the constrained environments.

An example of a manufacturing manipulation that requires compliancy is robotic assembly. To perform the assembly of parts that are not perfectly aligned, one must use a compliant element between the part and the robot to ease the insertion process. The RCC can be attached to the endpoint of the robot manipulators [3], [20]. This device develops a passive compliant interface between the robot and the part. The primary function of the RCC is to act as a filter that decreases the contact force between the part and the robot arising from the robot oscillations, robot programming error, and part fixturing errors. These end effectors are called passive because the elements that generate compliancy are passive and no external energy is flowing into the system.

Active end effectors are devices that can be mounted at the endpoint of the robot manipulators to develop more degrees of freedom [5]. This paper describes the design, construction, and control of an active end effector that can be used as a compliant tool holder. There is no passive compliant element in the system, because the compliancy in the system is generated electronically [6], [7], [11]. The advantage of this system over passive systems is that one can modulate the compliancy in the system arbitrarily by an on-line computer,

0882-4967/88/0600-0324$01.00

depending on the requirements of the tasks. Two dc actuators power the two degrees of freedom of the system.

II. Architecture

Fig. 1 shows the schematic diagram of the active end effector. The end effector is a 5-bar linkage with two degrees of freedom. All are articulated drive joints. The links are made of aluminum 6061. The actuators are dc brushless direct-drive motors equipped with 12-bit encoders and tachometers. The choice of the direct-drive system eliminates backlash and develops more structural rigidity in the system. This structural rigidity allows for a wide control bandwidth and higher precision. The stall torque and the peak torque for each motor is 5 lb·in and 20 lb·in, respectively. Each motor weighs 2.4 lb. A wide-bandwidth piezoelectric-based force sensor is located between the endpoint of the mechanism and the end-effector gripper to measure the force on the tool. The force sensor is preloaded by a clamping bolt, and measures the force in two dimensions in the plane of the mechanism. The entire weight of the links with bearings and force sensor is 111.4 g. The end effector can be attached to the robot manipulator by a simple fixture between the housing of the motors and the robot endpoint as shown in Fig. 2. Fig. 3 shows the side view of the end effector.

The characteristics of this end effector are as follows:

size of the 5-bar linkage at nominal position	2.167 in × 4.160 in
height of the end effector with motors (excluding the grinder tool)	3.760 in
linear workspace of the endpoint	0.3 in × 0.3 in
resolution of the endpoint motion	2.6×10^{-3} in
bandwidth of the control system	15 Hz
total mass of the mechanism (without the tool)	0.25 lb
weight of two motors	4.8 lb
weight of the tool	0.3 lb
total mass (mass of the mechanism and the motors, excluding the grinding tool)	5.05 lb.

Fig. 4 shows the size of the end effector relative to a hand.

III. Motivation for Development of the Active End Effector

This section explains briefly a practical problem that requires modulation of the compliance in the system by an on-line computer. This example also shows the limitation of passive RCC in developing a desired stiffness for arbitrary frequency ranges. The details of the problem are given in [8], [10].

Consider the deburring of a surface by a robot manipulator; the objective is to use an end effector to smooth the surface down to the commanded trajectory depicted by the dashed line in Fig. 5. It is intuitive to design a system with a large impedance (small compliance) in the normal direction and a small impedance (large compliance) in the tangential direction. We define impedance as the ratio of the contact force to the end-effector deflection as a function of frequency.

A large impedance in the normal direction causes the

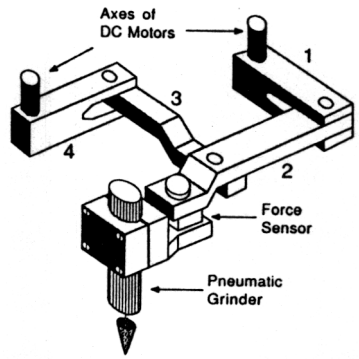

Fig. 1. The active end effector holding a pneumatic grinder.

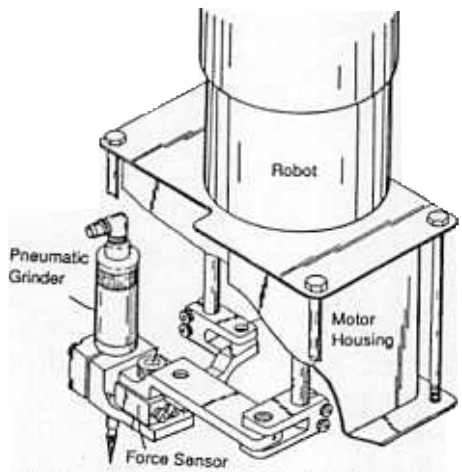

Fig. 2. The active end effector held by a robot.

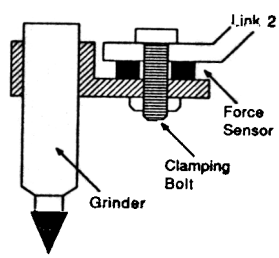

Fig. 3. The side view of the force sensor assembly.

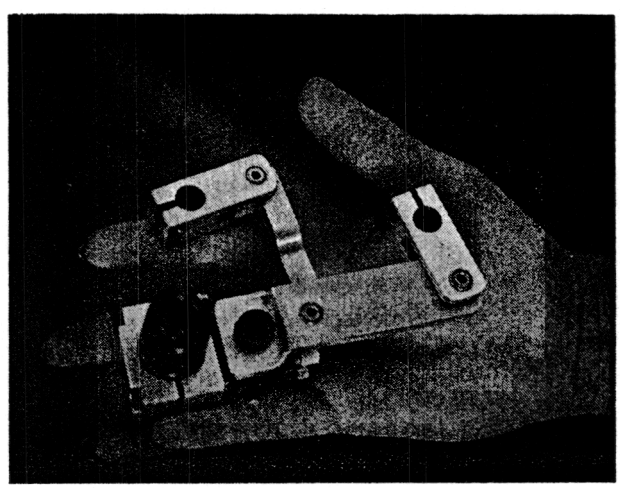

Fig. 4. The active end effector.

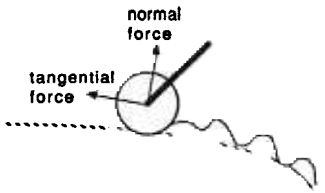

Fig. 5. Deburring an edge.

endpoint of the grinder to reject the interaction forces and stay very close to the commanded trajectory (dashed line). The larger the impedance of the end effector in the normal direction, the smoother the surface will be. Given the volume of the metal to be removed, the desired tolerance in the normal direction prescribes an approximate value for impedance in the normal direction. The force necessary to cut in the tangential direction at a constant traverse speed is approximately proportional to the volume of the metal to be removed [8]–[10]. Therefore, the larger the burrs on the surface, the slower the manipulator must move in the tangential direction to maintain a relatively constant tangential force. This is necessary because the slower speed of the endpoint along the surface implies a smaller volume of metal to be removed per unit of time, and consequently, less force in the tangential direction. To remove the metal from the surface, the grinder should slow down in response to contact forces with large burrs.

The above explanation demonstrates that it is necessary for the end effector to accommodate the interaction forces along the tangential direction, which directly implies a small impedance value in the tangential direction. If a designer does not accommodate the interaction forces by specifying a small stiffness value in the tangential direction, the large burrs on the surface will produce large contact forces in that direction and consequently stall the tool. Large contact forces in the tangential direction may develop a deflection in the endpoint position in the normal direction which might exceed the desired tolerance. A small value for the impedance in the tangential direction (relative to the impedance in the normal direction) guarantees small contact force in the tangential direction. The frequency spectrum of the roughness of the surface and the desired translational speed of the robot along the surface determine the *frequency range of operation*, ω_b.

On the other hand, for compensation of the robot oscillation, the impedance of the end effector in the normal direction must be small for all the frequency range of the robot oscillations and fixturing errors, ω_r. The small impedance (large compliance) in the normal direction allows for compensation of the robot position uncertainties and part-fixturing errors. Choosing a large impedance in the normal direction for deburring purpose conflicts with the required impedance to compensate for robot oscillations. The compensation for robot position uncertainties demands a low impedance (large compliance) in the normal direction, while a large impedance is required for deburring purposes. In theory, both requirements could be satisfied if one designs an end effector with the dynamic characteristics shown in Fig. 6. As shown in Fig. 6, $|\delta X_n(j\omega)/\delta F_n(j\omega)|$ is very large for the entire frequency range of the robot oscillations and the fixturing errors ω_r, and

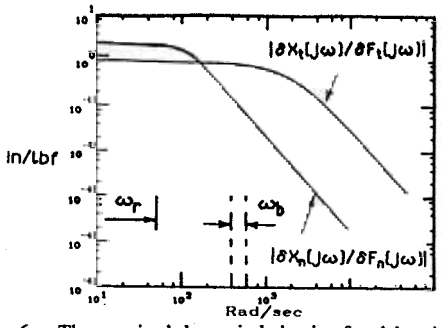

Fig. 6. The required dynamic behavior for deburring.

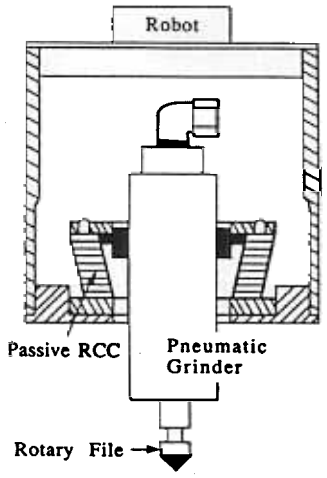

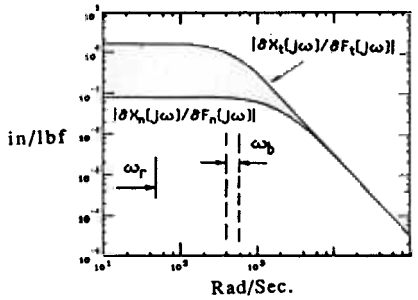

Fig. 7. A passive end effector and its dynamic behavior [2].

very small for the entire frequency range of the burr ω_b. While a large $|\delta X_n(j\omega)/\delta F_n(j\omega)|$ in $(0, \omega_r)$ does not let the robot oscillations develop a large variation in the normal contact force, a small $|\delta X_n(j\omega)/\delta F_n(j\omega)|$ in ω_b will cause the end effector to be very stiff in response to the burrs. Fig. 6 also shows the dynamic behavior of the end effector in the tangential direction. For all $\omega \in \omega_b$, $|\delta X_t(j\omega)/\delta F_t(j\omega)|$ is large to guarantee the deburring requirements. Note that $|\delta X_n(j\omega)/\delta F_n(j\omega)| \ll |\delta X_t(j\omega)/\delta F_t(j\omega)|$ for all $\omega \in \omega_b$.

It is *impossible* to design and build a passive end effector using a conventional RCC with the dynamic characteristics shown in Fig. 6. This is because of the role played by the constant mass of the tool in the dynamic behavior of the end effector. Fig. 7 shows a passive tool holder that contains an RCC [2]. Since the mass of the grinder is a constant parameter in the dynamic equations of the passive end effector in both

directions, the only possible dynamic behavior for a passive end effector is of the form given in Fig. 7. For a given set of K_n and K_t in both directions, one cannot choose arbitrary natural frequencies (or approximately bandwidth) in both directions. The natural frequencies (or bandwidths) for a passive end effector are fixed approximately at $\sqrt{K_n/M}$ and $\sqrt{K_t/M}$. Once K_n and K_t are chosen for deburring requirement and the compensation of the robot oscillation and the fixturing errors, then $\sqrt{K_n/M}$ and $\sqrt{K_t/M}$ cannot arbitrarily be chosen to meet the requirements of the ω_r and ω_b. Note that it is possible to build a passive end effector with dynamic behavior similar to the one in Fig. 6 if an orthogonal structure with independent springs is used in the design.

We will show in Section V that with the proposed active end effector one can modulate the impedance of the system electronically. This method is called impedance control [4], [6], [7], [11]. With this method one can choose arbitrary stiffness in two orthogonal directions, within two various frequency ranges.

IV. Design

In this section two significant properties of this end effector are explained. Although the active end effector can be used as a micropositioning system for small and fast maneuvering of the tool, it is designed to act as an RCC. The endpoint of the end effector behaves as if there were two orthogonal springs holding the tool. In this behavior, the endpoint motion is very small. Equation (1) describes the dynamic behavior of the mechanism, for small perturbation of the mechanism around its nominal point in absence of the centrifugal and Coriolis forces. We will justify the absence of centrifugal and Coriolis forces in the dynamic equations of the system in our analysis.

$$\ddot{X} = J_0 M_0^{-1} T \tag{1}$$

where

$X = [X_t\ X_n]^T$	2×1 vector of the tool position in the Cartesian coordinate frame,
J_0	2×2 Jacobian matrix,
M_0	2×2 mass matrix,
$T = [T_1\ T_2]^T$	2×1 vector of the motor torque.

$J_0 M_0^{-1}$ is a transmission ratio between the actuator torque and the endpoint acceleration. This matrix is a function of joint angles. It is desirable to operate the end effector in an orientation such that $J_0 M_0^{-1}$ is almost constant or has minimum rate of change. The general forms of M_0 and J_0 are given in the Appendix by (A1) and (A2). Fig. 19 in the Appendix shows a 5-bar linkage in the general form. The device is designed to operate around the neighborhood of the nominal orientation of $\theta_1 = 90°$, $\theta_2 = 0°$, $\theta_3 = 90°$, and $\theta_4 = 180°$ as shown in Fig. 8. θ_1 and θ_4 are the driving angles, and we intend to drive the system such that $85° < \theta_1 < 95°$ and $175° < \theta_4 < 185°$ (total of $\pm 5°$ deviation from their nominal values). It can be shown that the rate of change of $J_0 M_0^{-1}$ at this nominal orientation is minimum. The dynamic manipulability ω_d is defined as the square root of the multiplication of the maximum and minimum singular values

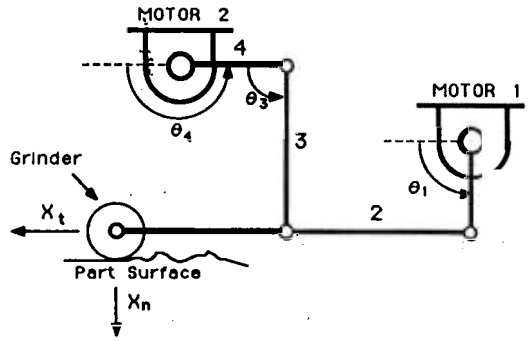

Fig. 8. The end effector at its nominal position $\theta_1 = 90°$ and $\theta_4 = 180°$

of $J_0 M_0^{-1}$ [19].[1] ω_d measures the rate of change of $J_0 M_0^{-1}$.

$$\omega_d = \sqrt{\sigma_{\max}(J_0 M_0^{-1})\,\sigma_{\min}(J_0 M_0^{-1})} \tag{2}$$

or equivalently

$$\omega_d = \sqrt{\det\,(J_0 M_0^{-1} M_0^{-T} J_0^T)}.$$

ω_d is plotted in Fig. 9 as a function of perturbations on $\delta\theta_1$ and $\delta\theta_4$. The perturbation around the nominal values of θ_1 and θ_4 are called $\delta\theta_1$ and $\delta\theta_4$. According to Fig. 9, ω_d is "smooth" for all small perturbations around nominal values of θ_1 and θ_4. Inserting $\theta_1 = 90°$, $\theta_2 = 0°$, $\theta_3 = 90°$, and $\theta_4 = 180°$ into (A1) and (A2) (from the Appendix) results in diagonal matrices for J_0 and M_0 such that $J_0 M_0^{-1}$ is diagonal and also has the minimum rate of change when θ_1 and θ_4 vary slightly from their nominal values. Note that the plot in Fig. 9 shows only that at the configuration shown, $J_0 M_0^{-1}$ has the minimum rate of change. This allows us to use (1) as our dynamic model for the active end effector. Since the rate of change of $J_0 M_0^{-1}$ is minimum at the nominal configuration, centrifugal and coriolis forces can be neglected from the dynamic equations of the end effector. (These terms are functions of the rate of change of the inertia matrix.) If the end effector is considered in another configuration, then any slight perturbation of the driving joints will develop significant change in $J_0 M_0^{-1}$ and, consequently, nonlinearity will be developed in the dynamic behavior of the system [1]. Since $J_0 M_0^{-1}$ is a diagonal matrix, then the dynamic equation of the end effector is uncoupled. Based on this uncoupling, for a limited range, motor 1 maneuvers the endpoint in the X_t direction, while motor 2 moves the endpoint independently in the X_n direction.

We use the end effector in the configuration shown in Fig. 8. All the links are orthogonal to one another. If θ_1 is perturbed from its nominal value as much as α, then the value of the endpoint perturbation in the X_n direction, δe, can be calculated form (3). Fig. 10 shows the configuration of the perturbed system.

$$\delta e = \frac{l_1}{2l_2}\,\alpha^2 \left(l_5 - l_2 - \frac{l_1 l_5}{l_3}\right) \tag{3}$$

[1] The maximum singular value of $J_0 M_0^{-1}$ is defined as

$$\sigma_{\max}(J_0 M_0^{-1}) = \max \frac{|J_0 M_0^{-1} z|}{|z|}$$

where z is a nonzero vector and $|\cdot|$ denotes the Euclidean norm.

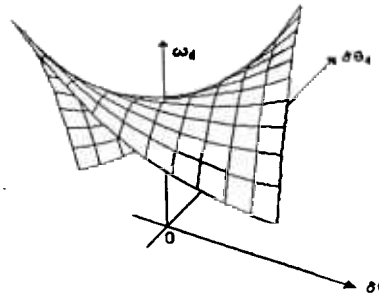

Fig. 9. Dynamic manipulability as a function of $\delta\theta_1$ and $\delta\theta_4$.

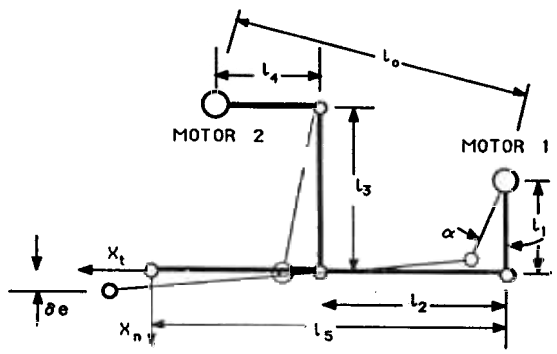

Fig. 10. The 5-bar mechanism with small deflection of α.

For $\delta e = 0$, the following equality must be satisfied:

$$l_5 - l_2 = \frac{l_1 l_5}{l_3}. \tag{4}$$

By satisfying (4), we choose the lengths of the mechanism such that the endpoint of the end effector always moves along the X_t axis for small value of $\alpha (\alpha < \pm 5°)$. This configuration is an application of the well-known Watts [12] straight line mechanism. This property is attractive for deburring purposes. According to [8], [10], the end effector must be very stiff in the direction normal to the part and compliant in the direction tangential to the part. Once the grinder encounters a burr, motor 1, which is responsible for motion in the X_t direction, moves the tool backward to decrease the amount of the force. In the deburring process, motor 1 constantly moves the endpoint back and forth in the X_t direction. If (4) is guaranteed, then the motion of the endpoint in the X_t direction does not affect the motion of the tool in the X_n direction. The following constraints are sufficient to result in the exact lengths of the mechanism:

- Equation (4) must be satisfied.
- For simplicity in design and construction, $l_1 = l_4$ and $l_3 = l_2$.
- $l_0 = 3$ in (each actuator has 1.375-in radius).
- l_4 must be such that if $\delta\theta_4 = 5°$, the amount of motion in the X_n direction is 0.15 in.

The above five constraints are sufficient conditions to acquire the lengths of the five links. Using the triangle equality and some algebra, the following lengths are calculated: $l_0 = 3$ in, $l_1 = 0.906$ in, $l_2 = 1.917$ in, $l_3 = 1.917$ in, and $l_4 = 0.906$ in.

V. Electronic Compliancy (Impedance Control)

First we frame the controller design objectives by a set of meaningful mathematical terms; then we give a summary of the controller design method to develop compliancy for linear systems. The complete description of the control method to develop electronic compliancy (impedance control) for a multi-degree-of-freedom nonlinear manipulative system is given in [9] and [11].

The controller design objective is to provide a stabilizing dynamic compensator for the system such that the ratio of the position of the endpoint of the end effector to an interaction force is constant within a given operating frequency range. (The very general definition is given in [6] and [7].) The above statement can be mathematically expressed by (5).

$$\delta F(j\omega) = K\delta X(j\omega), \qquad \text{for all } 0 < \omega < \omega_o \tag{5}$$

where

$\delta F(j\omega)$	2×1 vector of the deviation of the interaction forces from their equilibrium value in the global Cartesian coordinate frame;
$\delta X(j\omega)$	2×1 vector of the deviation of the endpoint position from the nominal point in the global Cartesian coordinate frame;
K	2×2 real-valued, nonsingular diagonal stiffness matrix with constant members;
ω_o	bandwidth (frequency range of operation);
j	complex number notation, $\sqrt{-1}$.

The stiffness matrix is the designer's choice which, depending on the application, contains different values for each direction. By specifying K, the designer governs the behavior of the end effector in constrained maneuvers. Large elements of the K matrix imply large interaction forces and torques. Small members of the K matrix allow for a considerable amount of motion in the end effector in response to interaction forces. Even though a diagonal stiffness matrix is appealing for the purpose of static uncoupling, the K matrix in general is not restricted to any structure.

Mechanical systems are not generally responsive to external forces at high frequencies. As the frequency increases, the effect of the feedback disappears gradually (depending on the type of controller used), until the inertia of the system dominates its overall motion. Therefore, depending on the dynamics of the system, (5) may not hold for a wide frequency range. It is necessary to consider the specification of ω_o as the second item of interest. In other words, two independent issues are addressed by (5): first, a simple relationship between $\delta F(j\omega)$ and $\delta X(j\omega)$; second, the frequency range of operation ω_o, such that (5) holds true. Besides choosing an appropriate stiffness matrix K, and a viable ω_o, a designer must also guarantee the stability of the closed-loop system. In summary, we are looking for a dynamic behavior for the manipulative system that resembles the dynamic behavior shown in Fig. 6.

We consider the architecture of Fig. 11 as the closed-loop control system for the end effector. The detailed description of each operator in Fig. 11 is given in [9] and [11]. Since the

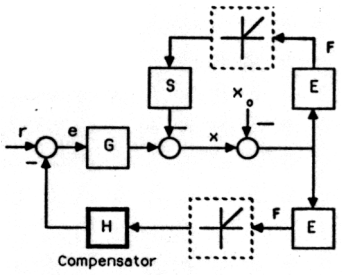

Fig. 11. The closed-loop control for the end effector.

dynamic behavior of the end effector in the neighborhood of its operating point is linear, all the operators in Fig. 11 are considered transfer function matrices. In the general approach for development of compliancy in [11], E, G, H, and S are nonlinear operators. G is the transfer function matrix that represents the dynamic behavior of the manipulative system (end effector in our case) *with a positioning controller*. The input to G is the vector of input trajectory e. The fact that most manipulative systems have some kind of positioning controllers is the motivation behind our approach. One can use a great number of methodologies for the development of the robust positioning controllers [14], [15], [18]. G can be calculated experimentally or analytically. Note that G is approximately equal to the unity matrix for the frequencies within its bandwidth. S is the sensitivity transfer function matrix. S represents the relationship between the external force on the endpoint of the end effector and the endpoint motion. This motion is due to either structural compliance in the end-effector mechanism or the positioning controller compliance. For a good positioning system S is quite "small." (The notion of "small" can be regarded in the singular value sense when S is a transfer function matrix. L_P-norm [18], [17] can be considered to show the size of S in the nonlinear case.) E represents the dynamic behavior of the environment. Readers can be convinced of the role of E by analyzing the relationship of the force and displacement of a spring as a simple model of the environment. H is the compensator to be designed. The input to this compensator is the contact force. The compensator output signal is being subtracted from the vector of input command r, resulting in the error signal e, as the input trajectory for the robot manipulator. r is the input command vector in the global coordinate frame which is used differently for the two categories of maneuvers; as a trajectory command to move the endpoint in unconstrained space and as a command to shape the contact force in the constrained space. When the manipulative system and environment are in contact, then the value of the contact force and the endpoint position are given by (6) and (7).

$$F=E(I+SE+GHE)^{-1}(Gr-X_0) \tag{6}$$

$$X=(I+SE+GHE)^{-1}(Gr-X_0). \tag{7}$$

The general goal is to choose a class of compensator H to shape the impedance of the system $E(I + SE + GHE)^{-1}G$ in (6). When the system is not in contact with the environment, the actual position of the endpoint is equal to the input trajectory command within the bandwidth of G. (Note that G is approximately equal to unity matrix within its bandwidth.) When the system is in contact with the environment, then the contact force follows r according to (6). We do not command any setpoint for force as we do in admittance control [13], [21]. This method is called Impedance Control [4], [6], [7] because it accepts a position vector as input and reflects a force vector as output. There is no hardware or software switch in the control system when the robot travels from unconstrained space to constrained space. The feedback loop on the contact force closes naturally when the robot encounters the environment. When the system is in contact with the environment, then the contact force is a function of r according to (6).

The compensator H must also guarantee the stability of the closed-loop system of Fig. 11. The general nonlinear sufficient condition for stability of the closed-loop system is given in [9] and [11]. The sufficient condition for stability of the linearly treated systems is given by inequality (8).

$$\sigma_{\max}(H) \leqslant \frac{1}{\sigma_{\max}(E(SE+I_n)^{-1}G)}, \qquad \text{for all } \omega \in (0, \infty). \tag{8}$$

If H is chosen outside of this class, instability and consequent separation may occur. Inequality (8) is a sufficient condition for stability. If inequality (8) is not satisfied, no conclusion on the stability of the system can be reached. Inequality (8) reveals some facts about the size of H. The smaller the sensitivity S, the smaller H must be chosen. Also, from inequality (8), the more rigid the environment, the smaller H must be chosen. In the "ideal case," no H can be found to allow a perfect positioning system ($S = 0$) to interact with an infinitely rigid environment ($E = \infty$).

In most manufacturing tasks such as robotic deburring, the endpoint of the manipulative system is in contact with a very stiff environment. We are interested in a particular case when $r = 0$. Suppose the environment is being moved into the end effector or the end effector is being moved into the environment as much as X_0. The relation between the contact force and the endpoint deflection is given by (9) if E approaches ∞ in the singular value sense.

$$F=(S+GH)^{-1}X_0. \tag{9}$$

Since G is a unity matrix for all $\omega \in (0, \omega_0)$, the value of the contact force F, within the bandwidth of the system $(0, \omega_o)$, can be approximated by (10).

$$F\approx(S+H)^{-1}X_0, \qquad \text{for all } \omega \in (0, \omega_o). \tag{10}$$

By knowing S and choosing H, one can shape the contact force. The value of $(S + H)$ within $(0, \omega_o)$ is the designer's choice and, depending on the task, it can have various values in different directions. A large value for $(S + H)$ within $(0, \omega_o)$ develops a compliant system while a small $(S + H)$ generates a stiff system. If H is chosen such that $(S + H)$ is "large" in the singular value sense at high frequencies, then the contact force in response to high-frequency components of r will be small. $(S + H)^{-1}$ is similar to the stiffness matrix, K which is defined by (5). By selecting the value of H and

knowledge of S one can select the members of H such that $(S + H)^{-1}$ of (10) meets the deburring requirements as given by (5). It is shown in [9] and [11] that the stability criterion for interaction with a very rigid environment is given by inequality (11).

$$\sigma_{\max}(H) \leqslant \frac{1}{\sigma_{\max}(S^{-1}G)}, \qquad \text{for all } \omega \in (0, \infty). \quad (11)$$

It is clear that if the environment is very rigid, then one must choose a very small H to satisfy the stability of the system when S is "small." (A good positioning system has "small" S.) Since G is a unity matrix for all $\omega \in (0, \omega_o)$, the bound for H, for a rigid environment and a "small" stiffness, is given by inequality (12).

$$\sigma_{\max}(H) \leqslant \sigma_{\min}(S), \qquad \text{for all } \omega \in (0, \omega_o). \quad (12)$$

If S is zero, then no H can be obtained to stabilize the system. In other words, to stabilize the system of the very rigid environment and the end effector, there must be a minimum compliancy in the end effector.

In general, for stability of the environment and a robot taken as a whole, there must be some initial compliancy either in the robot or in the environment. The initial compliancy in the robot can be obtained by a nonzero sensitivity function or a passive compliant element such as an RCC (Remote Center Compliance). Practitioners always observed that the system of a robot and a stiff environment can always be stabilized when a compliant element (e.g., piece of rubber or an RCC) is installed between the robot and environment. One can also stabilize the system of robot and environment by increasing the robot sensitivity function. In many commercial manipulators the sensitivity of the robot manipulators can be increased by decreasing the gain of each actuator positioning loop. This also results in a narrower bandwidth (slow response in the unconstrained maneuvering) for the robot positioning system.

VI. Experiments

Two sets of experiments are described here to present the dynamic behavior of the end effector in constrained and unconstrained maneuvering. In Section VI-A, the experimental frequency response of the transfer function matrix G and the sensitivity transfer function matrix S are given. The values of G and S are necessary to estimate the stability bound on H. Section VI-B demonstrates the endpoint impedance $(S + H)^{-1}$ and the uncoupled time-domain closed-loop dynamic behavior of the end effector in the constrained and unconstrained maneuvering. The control architecture of Fig. 11 is used to control the system.

Two brushless dc motors are used to power the two degrees of freedom of the end effector. The continuous stall torque and peak torque are 5 lbf-in and 20 lbf-in at 2.25 and 6.7 A, respectively. Motors are driven by two PWM amplifiers. The amplifier has 7.5-A continuous output current. Both motors are equipped with resolvers that provide 12-bit orientation data and an analog velocity feedback signal with resolution of 0.019 V/rad/s. A two-component piezoelectric force transducer and a charge amplifier are used to measure forces in two directions in the Cartesian coordinate frame. The force transducer is preloaded at the endpoint of the end effector by a clamping screw as shown in Fig. 3. The resolution of the force transducer is 2.2×10^{-3} lbf. The stiffness of the force transducer in each measuring direction is about 1.5×10^{9} lbf/in.

Since the dynamic behavior of the end effector in two directions is uncoupled, matrices E, S, G, and H of Fig. 11 are diagonal. Each motor of the end effector was treated separately and a control loop similar to the one in Fig. 11 was designed for each motor.

A. Experimental and Theoretical Values of G and S

In this set of experiments, the position transfer function matrix G and the sensitivity transfer function S are measured. Fig. 12 shows the analytical and experimental values of G for two orthogonal directions. For measuring G, a series of sinusoidal commands with frequencies within 15 Hz were imposed on each motor.

The amplitude of orientation of each motor was measured at each frequency. The ratio of the rotation of the motor to the input command represents the magnitude of G at each frequency. For measurement of the sensitivity transfer function matrix, the input excitation was supplied by the rotation of an eccentric mass mounted on the tool bit. Fig. 13 shows the experimental setup for measurement of S. The rotating mass exerts a centerifugal, sinusoidal force on the tool bit. The frequency of the imposed force is equal to the frequency of rotation of the mass. By varying the frequency of the rotation of the mass, one can vary the frequency of the imposed force on the end effector. Fig. 14 depicts the sensitivity transfer function. The values of the sensitivity transfer functions along the normal and tangential directions, within their bandwidths, are 0.7 in/lbf and 0.197 in/lbf, respectively.

B. The Closed-Loop Dynamic Behavior of the End Effector

Frequency-domain and time-domain methods have been used to describe the dynamic behavior of the closed-loop system. Section VI-B1 is devoted to verifying experimentally the model of the endpoint compliancy in both directions when an H is designed to close the loop as shown in Fig. 11.

1) The Endpoint Compliancy: The nature of compliancy for the end effector is given by (9). H was chosen such that $(S + H)^{-1}$ in each direction is equal to the desired stiffness given by (5). H must also guarantee the stability of the closed-loop system. The stability criterion for a one-degree-of-freedom system is given by inequality (13).

$$|HG| < |(S + 1/E)|, \qquad \text{for all } \omega \in (0, \infty) \quad (13)$$

where $|\cdot|$ denotes the magnitude of a transfer function. Since in many cases $G \approx 1$ for all $0 < \omega < \omega_o$, then H must be chosen such that the following inequality is satisfied:

$$|H| < |(S + 1/E)|, \qquad \text{for all } \omega \in (0, \omega_o). \quad (14)$$

Inequality (14) shows that the more rigid the environment, the smaller H must be chosen to guarantee the stability of the

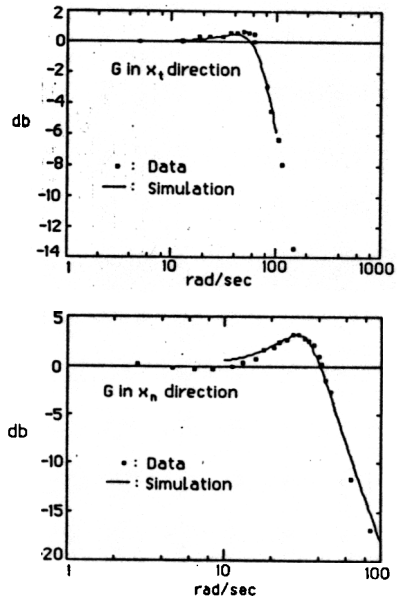

Fig. 12. The position transfer function G.

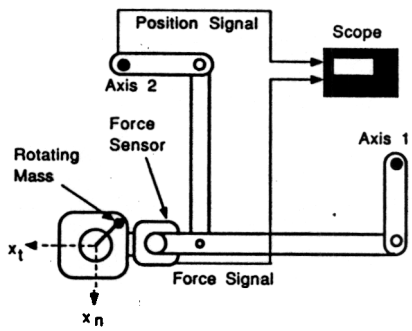

Fig. 13. The experimental setup for measurement of the sensitivity transfer function.

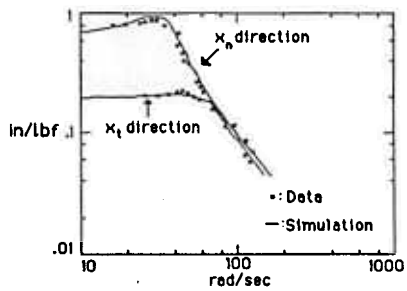

Fig. 14. The sensitivity transfer function S.

closed-loop system. In the case of a rigid environment ("large" E) and a "good" positioning system, H must be chosen as a very small gain. The values for H along the normal and tangential directions within their bandwidths are 0.01 and 0.194 in/lbf, respectively. These values result in 0.39 and 0.7 in/lbf for $(S + H)$ within the bandwidth of the system. The values of $(S + H)$ within its bandwidth represent the members of matrix K^{-1} in (5). Fig. 15 shows the experimental and theoretical values of the endpoint compliancy (Fig. 15 actually shows the endpoint admittance where it is reciprocal of the impedance in the linear case.) The experimental setup shown in Fig. 13 was used to measure the

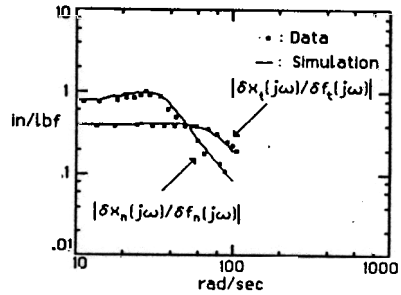

Fig. 15. The endpoint admittance (1/impedance).

endpoint compliancy. The dynamic behavior of Fig. 15 can be compared with the desired dynamic response for deburring given by Fig. 6.

2) Uncoupling of the Contact Forces: In this set of experiments, the whole end effector was moved in two different directions to encounter an edge of a part. The objective was to observe the uncoupled time-domain dynamic behavior of the end effector when the end effector is in contact with the hard environment. The controller was designed according to [11] such that K_t and K_n are 0.32 and 4.0 lb/in, respectively. First, the end effector was moved 0.5 in beyond the edge of the part in the X_n direction. Fig. 8 shows the schematics of the setup.

Fig. 16 shows the contact forces. The force in the X_n direction increases from zero to 2.0 lbf while the force in the X_t direction remains at zero. Next, the end effector was moved 0.5 in beyond the edge of the part in the X_t direction. Fig. 17 shows the contact forces. The force in the X_t direction increases from zero to 0.16 lbf while the force in the X_n direction remains at zero. In both cases, the end effector was moved 0.5 in beyond the edge of the stiff wall. Since the stiffness of the end effector in the X_n direction is larger than the stiffness in the X_t direction, the contact force in the X_n direction is larger than the contact force in the X_t direction.

3) Uncoupling of the Motion: The objective was to observe the uncoupled dynamic behavior of the end effector in unconstrained maneuvering of the end effector when (4) is satisfied. The endpoint of the end effector was ordered to move in the X_t direction. Fig. 18 shows the joint angles, θ_1 and θ_4, of the end effector when θ_1 is accepting a step-wise motion command. θ_4 remains at 180°. The plot shows the uncoupling of the joint angles in the closed-loop system.

VII. Summary and Conclusion

An active end effector with controllable, compliant motion (Electronic Compliancy) has been designed, built, and tested for robotic operations. The active end effector (unlike the passive system) does not contain any spring or dampers. The compliancy in the active end effector is developed electronically and therefore can be modulated by an on-line computer. The active end effector allows for compensation of the robot's position uncertainties from fixturing errors, robot programing resolution, and robot oscillations. This fully instrumented end effector weighs only 5.05 lb and can be mounted at the endpoint of the commercial robot manipulator. Two state-of-the-art miniature actuators power the end effector directly. The high stiffness and light weight of the material used in the

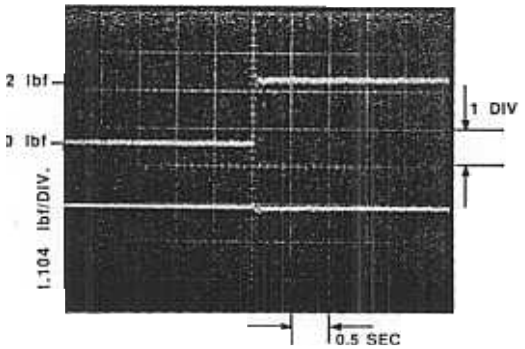

Fig. 16. Force in the X_n direction increases from zero to 2 lbf.

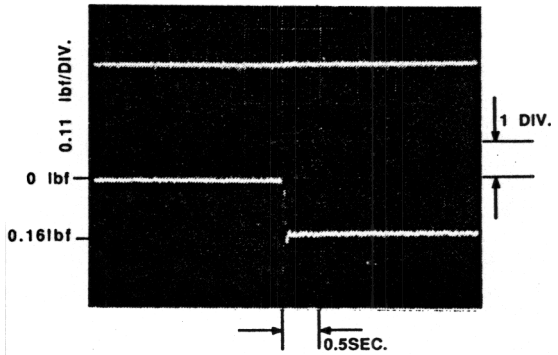

Fig. 17. Force in the X_t direction increases from zero to 0.16 lb.

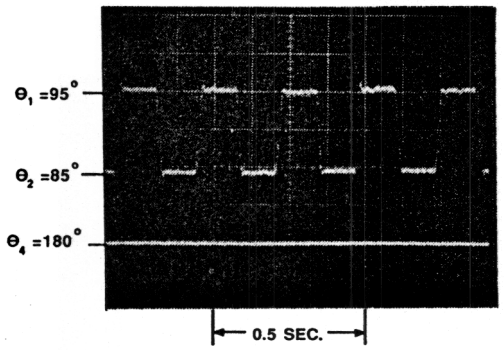

Fig. 18. Uncoupled motion in two orthogonal directions.

system allows for a wide-bandwidth impedance control. A miniature force cell measures the forces in two dimensions. The tool holder can maneuver a very light pneumatic grinder in a linear workspace of about 0.3 in × 0.3 in. The measurements taken on the mechanism are contact forces, angular velocities, and the orientation of the mechanism. Satisfying a kinematic constraint for this end effector allows for uncoupled dynamic behavior for a bounded range.

Appendix

This Appendix is dedicated to deriving of the Jacobian and the mass matrix of a general 5-bar linkage. In Fig. 19, j_i, l_i, x_i, m_i, and θ_i represent the moment of the inertia relative to the endpoint, length, location of the center of mass, mass, and the orientation of each link for $i = 1, 2, 3$, and 4.

Using the standard method, the Jacobian of the linkage can

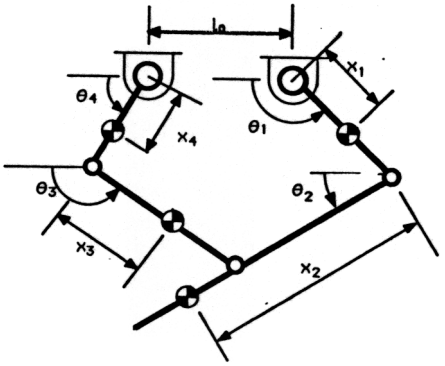

Fig. 19. The 5-bar linkage in the general form.

be represented by (A1)

$$J_0 = \begin{bmatrix} J_{11} & J_{12} \\ J_{21} & J_{22} \end{bmatrix}$$

where

$$J_{11} = -l_1 \sin(\theta_1) + al_5 \sin(\theta_2)$$

$$J_{21} = l_1 \cos(\theta_1) - al_5 \cos(\theta_2)$$

$$J_{12} = -bl_5 \sin(\theta_2)$$

$$J_{22} = bl_5 \cos(\theta_2).$$

The mass matrix is given by (A2)

$$M = \begin{bmatrix} M_{11} & M_{12} \\ M_{21} & M_{22} \end{bmatrix}$$

where

$$M_{11} = j_1 + m_2 l_1^2 + j_2 a^2 + j_3 c^2 + 2x_2 l_1 \cos(\theta_1 - \theta_2) am_2$$

$$M_{12} = j_2 ab + b \cos(\theta_1 - \theta_2) x_2 l_1 m_2 + j_3 cd + c \cos(\theta_4 - \theta_3) x_3 l_4 m_3$$

$$M_{21} = M_{12}$$

$$M_{22} = 2m_3 l_4 x_3 d \cos(\theta_4 - \theta_3) + j_3 d^2 + j_4 + m_3 l_4^2 + j_2 b^2.$$

a, b, c, and d are given below.

$$a = l_1 \sin(\theta_1 - \theta_3)/(l_2 \sin(\theta_2 - \theta_3))$$

$$b = l_4 \sin(\theta_4 - \theta_3)/(l_2 \sin(\theta_2 - \theta_3))$$

$$c = l_1 \sin(\theta_1 - \theta_2)/(l_3 \sin(\theta_2 - \theta_3))$$

$$d = l_4 \sin(\theta_4 - \theta_2)/(l_3 \sin(\theta_2 - \theta_3)).$$

References

[1] H. Asada and K. Youcef-Toumi, "Analysis and design of a direct drive arm with a five-bar-link parallel drive mechanism," *ASME J. Dynamic Syst., Meas., Contr.*, vol. 106, no. 3, pp. 225-230, 1984.

[2] J. Bausch, B. Kramer, and H. Kazerooni, "The development of the compliant tool holders for robotic deburring," presented at the ASME Winter Annual Meet., Anaheim, CA, Dec. 1986.

[3] S. H. Drake, "Using compliance in lieu of sensory feedback for automatic assembly," presented at the IFAC Symp. on Information and Control Problems in Manufacturing Technology, Tokyo, Japan, 1977.

[4] N. Hogan, "Impedance control: An approach to manipulation, Part 1: Theory, Part 2: Implementation, Part 3: Applications," *ASME J. Dynamic Syst., Meas., Contr.*, 1985.
[5] R. L. Hollis, "A planar XY robotic fine positioning device," in *Proc. IEEE Int. Conf. on Robotics and Automation* (St. Louis, MO, Mar. 1985).
[6] H. Kazerooni, P. K. Houpt, and T. B. Sheridan, "Fundamentals of robust compliant motion for manipulators," *IEEE J. Robotics Automat.*, vol. RA-2, no. 2, pp. June 1986.
[7] ——, "A design method for robust compliant motion of manipulators," *IEEE J. Robotics Automat.*, vol. RA-2, no. 2, pp. June 1986.
[8] H. Kazerooni, J. J. Bausch, and B. Kramer, "An approach to automated deburring by robot manipulators," *ASME J. Dynamic Syst., Meas., Contr.*, Dec. 1986.
[9] H. Kazerooni, "On the stability of the robot compliant motion control," in *Proc. 26th IEEE Conf. on Decision and Control* (Los Angeles, CA, Dec. 1987).
[10] ——, "Automated robotic deburring using electronic compliancy; impedance control," in *Proc. IEEE Int. Conf. on Robotics and Automation* (Raleigh, NC, Mar. 1987).
[11] ——, "Non-linear robust impedance control for robot manipulators," in *Proc. IEEE Int. Conf. on Robotics and Automation* (Raleigh, NC, Apr. 1987).
[12] S. Rappaport, "Five-bar linkage for straight line motion," *Product Eng.*, Oct. 1959.
[13] M. H. Raibert and J. J. Craig, "Hybrid position/force control of manipulators," *ASME J. Dynamic Syst., Meas., Contr.*, June 1981.
[14] J. J. Slotine, "Sliding controller design for non-linear systems," *Int. J. Contr.*, vol. 40, no. 2, 1984.
[15] ——, "The robust control of of robot manipulators," *Int. J. Robot. Res.*, vol. 4, no. 2, 1985.
[16] M. Vidyasagar, *Non-Linear Systems Analysis*. Englewood Cliffs, NJ: Prentice-Hall, 1978.
[17] C. A. Desoer and M. Vidyasagar, *Feedback Systems: Input-Output Properties*. New York, NY: Academic Press, 1975.
[18] M. Vidyasagar and W. M. Spong, "Robust non-linear control of robot manipulators," presented at the IEEE Conf. on Decision and Control, Dec. 1985.
[19] T. Yoshikawa, "Dynamic manipulability of robot manipulators," *J. Robotic Syst.*, vol. 2, no. 1, 1985.
[20] P. C. Watson, "A multidimensional system analysis of the assembly process as performed by a manipulator," in *Proc. Ist Amer. Robot Conf.* (Chicago, IL, 1976).
[21] D. E. Whitney, "Force-feedback control of manipulator fine motions," *ASME J. Dynamic Syst., Meas., Contr.*, June 1977.

H. Kazerooni was born in Tehran, Iran, in May 1956. He received the M.S. degree in mechanical engineering from the University of Wisconsin, Madison, in 1980, and the M.S.M.E. and Sc.D. degrees in mechanical engineering from the Man-Machine Systems Laboratory of the Massachusetts Institute of Technology, Cambridge, in 1982 and 1984, respectively.

From 1984 to 1985, he was with the Laboratory of Manufacturing and Productivity at the Massachusetts Institute of Technology as a Post Doctoral Fellow. He is currently Assistant Professor in Mechanical Engineering Department at the University of Minnesota, Minneapolis.